

Accepted for publication in *The Astrophysical Journal*

The Unusual Infrared Object HDF–N J123656.3+621322^{1,3}

MARK DICKINSON² AND CHRISTOPHER HANLEY

Space Telescope Science Institute, 3700 San Martin Dr., Baltimore MD 21218

RICHARD ELSTON²

Department of Astronomy, University of Florida, Gainesville, FL, 32611

PETER R. EISENHARDT²

MS 169-327, Jet Propulsion Laboratory, California Institute of Technology, 4800 Oak Grove Drive, Pasadena, CA, 91109

S. A. STANFORD²

University of California at Davis, and the Institute of Geophysics and Planetary Physics, Lawrence Livermore National Laboratories, Livermore, CA, 94550

KURT L. ADELBERGER, ALICE SHAPLEY, AND CHARLES C. STEIDEL

Palomar Observatory, Caltech 105–24, Pasadena, CA 91125

CASEY PAPOVICH AND ALEXANDER S. SZALAY

Department of Physics and Astronomy, The Johns Hopkins University, 3400 N. Charles St., Baltimore MD 21218

MATTHEW A. BERSHADY² AND CHRISTOPHER J. CONSELICE

Department of Astronomy, University of Wisconsin, 475 N. Charter St., Madison, WI 53706

HENRY C. FERGUSON AND ANDREW S. FRUCHTER

Space Telescope Science Institute, 3700 San Martin Dr., Baltimore MD 21218

¹Based on observations with the NASA/ESA Hubble Space Telescope, obtained at the Space Telescope Science Institute, which is operated by the Association of Universities for Research in Astronomy, Inc., under NASA contract NAS5-26555.

²Visiting Astronomer, Kitt Peak National Observatory, National Optical Astronomy Observatories, which is operated by the Association of Universities for Research in Astronomy, Inc. (AURA) under cooperative agreement with the National Science Foundation.

³Partially based on data obtained at the W.M. Keck Observatory, operated as a scientific partnership among the California Institute of Technology, the University of California, and NASA, and made possible by the generous financial support of the W.M. Keck Foundation.

ABSTRACT

We describe an object in the Hubble Deep Field North with very unusual near-infrared properties. It is readily visible in *Hubble Space Telescope* NICMOS images at $1.6\mu\text{m}$ and from the ground at $2.2\mu\text{m}$, but is undetected (with signal-to-noise $\lesssim 2$) in very deep WFPC2 and NICMOS data from 0.3 to $1.1\mu\text{m}$. The f_ν flux density drops by a factor $\gtrsim 8.3$ (97.7% confidence) from 1.6 to $1.1\mu\text{m}$. The object is compact but may be slightly resolved in the NICMOS $1.6\mu\text{m}$ image. In a low-resolution, near-infrared spectrogram, we find a possible emission line at $1.643\mu\text{m}$, but a reobservation at higher spectral resolution failed to confirm the line, leaving its reality in doubt. We consider various hypotheses for the nature of this object. Its colors are unlike those of known galactic stars, except perhaps the most extreme carbon stars or Mira variables with thick circumstellar dust shells. It does not appear to be possible to explain its spectral energy distribution as that of a normal galaxy at any redshift without additional opacity from either dust or intergalactic neutral hydrogen. The colors can be matched by those of a dusty galaxy at $z \gtrsim 2$, by a maximally old elliptical galaxy at $z \gtrsim 3$ (perhaps with some additional reddening), or by an object at $z \gtrsim 10$ whose optical and $1.1\mu\text{m}$ light have been suppressed by the intergalactic medium. Under the latter hypothesis, if the luminosity results from stars and not an AGN, the object would resemble a classical, unobscured protogalaxy, with a star formation rate $\gtrsim 100M_\odot \text{ yr}^{-1}$. Such UV-bright objects are evidently rare at $2 < z < 12.5$, however, with a space density several hundred times lower than that of present-day L^* galaxies.

Subject headings: early universe — galaxies: photometry — galaxies: evolution — infrared: galaxies

1. Introduction

In recent years, astronomers have extensively developed the art of selecting interesting, high redshift objects on the basis of their broad band colors. Color selection has long been used to separate distant quasar candidates from the multitude of foreground stars either via their UV excess (e.g., Veron 1983) or by color criteria based on the passage of the 1216Å Lyman α forest and 912Å Lyman limit discontinuities through broad passbands (e.g., Warren *et al.* 1987). Guhathakurta, Tyson, & Majewski (1990) applied the latter technique to search for high redshift galaxies, and the method was brought to fruition by Steidel *et al.* (1996a,b, 1999) who have successfully identified and spectroscopically confirmed nearly 1000 galaxies at $2 < z < 4.5$ using this approach. Other interesting classes of objects have been selected and studied on the basis of having extremely red optical-to-infrared colors (e.g., Elston, Rieke, & Rieke 1988, 1989; Hu & Ridgway 1994; Graham & Dey 1996; Thompson *et al.* 1999). Some of these turn out to be early type galaxies at high redshift, while others are both distant and dust-obscured. In general, estimating galaxy redshifts from broad band colors is now a popular industry, and much progress has been made in applying such techniques at intermediate redshifts (e.g., Brunner, Connolly & Szalay 1999) and for identifying candidates for extremely distant galaxies (Lanzetta, Yahil, & Fernández-Soto 1996). Indeed, some of the most distant galaxies now known have been found in this way (e.g., HDF 4-473, Weymann *et al.* 1998; HDF 3-951, Spinrad *et al.* 1998⁴).

The Hubble Deep Fields (North and South, or HDF-N and HDF-S, Williams *et al.* 1996 and 1999) have been valuable data sets for exploring such techniques because of the extremely deep, multiwavelength data which are available. We have recently mapped the complete HDF-N in the near-infrared with NICMOS on board the *Hubble Space Telescope* (HST). These data offer new opportunities for identifying interesting objects on the basis of their colors. Here we describe an object with perhaps the most unusual colors in the HDF-N, which is significantly detected only at $\lambda \geq 1.6\mu\text{m}$. We discuss our imaging and spectroscopic observations of this object, and consider various interpretations of its nature.

2. Imaging and Photometry

We observed the HDF-N with NICMOS (Thompson *et al.* 1998) between UT 1998 June 13 and June 23, during the second refocus campaign when the HST secondary mirror was moved to ensure optimal focus for NICMOS Camera 3. The observations and data reduction will be described in detail elsewhere (Dickinson *et al.*, in preparation); the immediately relevant aspects are summarized here. The complete HDF-N was mosaiced with 8 sub-fields, each imaged during three separate visits. During each visit, exposures were taken through both the F110W ($1.1\mu\text{m}$) and F160W ($1.6\mu\text{m}$) filters. (Henceforth we will refer to the six WFPC2 and NICMOS HDF

⁴We will occasionally use catalog numbers from Williams *et al.* 1996 to identify HDF galaxies in this paper.

bandpasses as U_{300} , B_{450} , V_{606} , I_{814} , J_{110} and H_{160} .) Each section of the mosaic was dithered through 9 independent positions, with a net exposure time of 12600s per filter, except in a few cases where telescope tracking was lost due to HST Fine Guidance Sensor failures. The region of interest for this paper did not lose any exposure time. The data were processed using a combination of STScI pipeline routines and custom software, and were combined into a single mosaic, accurately registered to the HDF–N WFPC2 images, using the “drizzling” method of Fruchter & Hook (1999). The NICMOS images have a point spread function (PSF) with FWHM $\approx 0''.22$, primarily limited by the pixel scale ($0''.2$) of Camera 3. Sensitivity varies over the field of view due to variations in NICMOS quantum efficiency and exposure time, but on average the images have a signal-to-noise ratio $S/N \approx 10$ within an $0''.7$ diameter aperture at $AB \approx 26.1$ for both the J_{110} and H_{160} filters.⁵ In order to ensure properly matched photometry between the optical and infrared images, the WFPC2 data were convolved to match the NICMOS PSF. Photometric catalogs were constructed using SExtractor (Bertin & Arnouts 1996), by detecting objects in the NICMOS images and measuring fluxes through matched apertures in all bands.

We first noticed the object which we will call HDF–N J123656.3+621322, or HDFN–JD1 for brevity, during a visual inspection of the NICMOS data for objects with unusual colors. It is prominent at $1.6\mu\text{m}$, but apparently invisible through all other HST filters, including J_{110} (Figure 1). Figure 2 shows a $J_{110} - H_{160}$ vs. H_{160} color–magnitude diagram highlighting the object’s extreme and unusual color. In $J_{110} - H_{160}$, HDFN–JD1 is by far the reddest among the ~ 1700 objects detected in our NICMOS survey.

Careful inspection of the NICMOS data convinces us that this is a real astronomical source, not an artifact, and that there is no evidence that it is transient or variable. It is visible in each of the nine individual, dithered H_{160} exposures, which were taken during telescope visits on UT 1998 June 16, 20 and 22–23, but is not detected in any of the corresponding J_{110} exposures taken during those same visits. We know of no NICMOS anomaly or optics ghost which could produce an artifact resembling what we observe.⁶ Moreover, the object is detected in two independent, ground–based near–IR data sets. It is faintly visible ($S/N \approx 4$) in the K_s ($2.16\mu\text{m}$) HDF images which we obtained with the KPNO 4m telescope in 1996 April–May (cf. Dickinson 1998). In fact, HDFN–JD1 is the brightest of the five “ K –band only” candidates identified in our KPNO 4m IR HDF images by Lanzetta, Yahil, & Fernández–Soto (1998). Their other four candidates have no counterparts in the NICMOS data.

To verify the K_s detection and to improve the quality of the photometry, we obtained new K_s images using NIRC (Matthews & Soifer 1994) on the Keck I telescope on UT 1999 April 5. 108 dithered 60 second exposures were taken through light, intermittent cirrus and processed

⁵Unless otherwise stated, we use AB magnitudes throughout this paper, defined as $AB = 31.4 - 2.5 \log\langle f_\nu \rangle$, where $\langle f_\nu \rangle$ is the flux density in nJy averaged over the filter bandpass.

⁶One NICMOS anomaly, the “Mr. Staypuft Effect” (cf. Skinner *et al.* 1998), produces electronic ghost images, but these are always offset by 128 pixels from brighter sources, which is not the case here.

using the DIMSUM⁷ reduction software. The individual frames were scaled and weighted before combination using measured counts of a moderately bright, nearby star centered in the NIRC field. The combined image has a PSF FWHM = 0".5. The photometric zeropoint was bootstrapped from the IRIM K_s data using large aperture measurements of two stars, which gave excellent internal agreement. HDFN–JD1 is readily visible as a compact source in the NIRC image (Figure 1).

We summarize photometry of the object in Table 1. In order to set limits in the HST bands U_{300} through J_{110} , we measured fluxes in a 0".7 diameter circular aperture at the H_{160} centroid position. This aperture maximizes S/N for the object in the H_{160} image, and is very close to that required to maximize S/N for point sources. We also have verified that the optical measurements in Table 1 are consistent with limits derived from the original, unconvolved WFPC2 images. A 21% aperture correction, derived from the H_{160} image, has been applied to the measurements, errors and limits in all HST bands to adjust the fluxes to “total” values. This correction assumes that the object has similar morphology at all wavelengths, which cannot be verified at present. We followed a similar procedure for the NIRC K_s image, using photometry measured within a 1".2 diameter aperture, corrected to total flux using curve of growth measurements of the reference star. We also measured the object in the IRIM K_s image using a method based on that of Fernández–Soto, Lanzetta & Yahil (1999). The NICMOS image is used as a template, convolved to match the IRIM PSF, and then fit to the ground–based data. The NIRC and IRIM measurements ($K_{AB} = 23.9$ and 23.8, respectively) agree within their errors, and with the value measured by Lanzetta *et al.* (1998) ($K_{AB} = 23.7$) from the same IRIM data. The 1σ and 2σ color limits for $J_{110} - H_{160}$ are >2.8 and >2.3 , respectively, while $H_{160} - K_s = 1.23^{+0.23}_{-0.19}$.

HDFN–JD1 has $S/N < 2$ in all bands other than H_{160} and K_s , regardless of the aperture size used. However, we do measure formally positive counts above the background at B_{450} , V_{606} , I_{814} and J_{110} . Although measurements at low significance levels are prone to systematic uncertainties in background subtraction, etc., there is nevertheless the possibility that the object does have non–zero optical flux. To explore this further, we have used an additional 63000s WFPC2 I_{814} image of the HDF obtained by Gilliland, Nugent, & Phillips (1999) in a search for high redshift supernovae. R. Gilliland kindly provided his sum of all available HDF–N I_{814} data in the WF3 region, with a total exposure time of 186600s. We registered this image with the data in other bandpasses. Photometry on the unconvolved, “grand sum” I_{814} image in an 0".7 aperture centered at the nominal position of JD1 measures a flux of 5.7 ± 2.6 nJy (with no aperture correction), or a formal $S/N = 2.2$.

To assess the significance of this optical measurement, we carried out a simple fluctuation analysis on the WFPC2 data. The images were normalized to constant variance over the field of view by dividing by smoothed noise maps which are generated as part of the data reduction process. We used SExtractor to generate masks which exclude all readily detectable sources in

⁷Deep Infrared Mosaicing Software, a package of IRAF scripts by Eisenhardt, Dickinson, Stanford and Ward, available at <ftp://iraf.noao.edu/contrib/dimsumV2>.

each image, including generous buffer regions around each. We fit smooth background maps to the “blank sky” regions and subtracted them from the images. The data were filtered by a Gaussian with $\text{FWHM} = 0''.14$ (matching the WFPC2 PSF), and the distribution of pixel values over an 855 arcsec^2 region was compared to that near the position of HDFN–JD1. We did this for each WFPC2 image, for variance weighted sums of the optical bandpasses, and also for χ^2 combinations constructed following the procedure of Szalay, Connolly, & Szokoly (1999). The results from the χ^2 images were statistically similar to those from the weighted sums, so we describe only the latter here. The filtered pixel values have a nearly Gaussian distribution (whose width in a given image we will characterize as σ here), with a positive tail due to faint sources. At the nominal JD1 peak position, the filtered I_{814} image has a value which exceeds the local background by 1.6σ , and in the weighted $V_{606} + I_{814}$ image by 1.9σ . There is a stronger local peak in the filtered I_{814} and $V_{606} + I_{814}$ images located $0''.14$ from the nominal JD1 position, which exceeds the local background by 3.1σ in I_{814} and by 3.3σ in $V_{606} + I_{814}$. Including the B_{450} data in the weighted sums or χ^2 images does not strengthen the peak. Its formal significance depends on how one treats the non–Gaussian tail of positive pixel values due to faint sources. Excluding buffered regions around all objects detected in the infrared catalogs, we find that there is a 5.1% chance of a pixel in the filtered $V_{606} + I_{814}$ images exceeding this “ 3.3σ ” threshold within $0''.14$ of a location specified *a priori*. The infrared catalogs, however, miss faint blue galaxies which are readily visible in the optical data, and which contribute to this positive tail. Excluding all objects detected in the infrared *or* optical SExtractor catalogs, the chance probability drops to 1.8%. The exact probabilities depend on the detection threshold used for the catalogs. We conclude that the optical “detection” corresponds to a Gaussian significance of 1.6 to 2.2σ .

HDFN–JD1 is not detected in the VLA radio maps of Richards *et al.* (1998) and Richards (1999), with a 3σ limit of $4.8\mu\text{Jy}$ at 8.5 GHz and $22.5\mu\text{Jy}$ at 1.4 GHz. It is not reported as a source in the ISO HDF catalogs of Goldschmidt *et al.* (1997), Aussel *et al.* (1999) or Désert *et al.* (1999), with approximate flux limits of $50\mu\text{Jy}$ and $25\mu\text{Jy}$ at 7 and $15\mu\text{m}$,⁸ nor as an $850\mu\text{m}$ source in the SCUBA observations of Hughes *et al.* (1998), with a limit of 2.0 mJy (4.4σ). Interestingly, the next reddest HDF object, J123651.74+621221.4 (with $J_{110} - H_{160} = 1.6$, $H_{160} = 24.3$; see Figure 2), corresponds to a VLA/MERLIN radio source, and may also have a $15\mu\text{m}$ counterpart in the Aussel *et al.* (1999) ISO source list, as well as a possible 3σ detection in the 1.3mm map of Downes *et al.* (1999).

3. Spectroscopy

We observed HDFN–JD1 using the Cryogenic Spectrograph (CRSP; Joyce 1995) at the KPNO 4m on UT 1999 May 2, 3, 6 and 7. We acquired the target using a blind offset from a

⁸These ISO flux limits are estimated based on measurements reported by Aussel *et al.* (1999) for two other “supplemental” $15\mu\text{m}$ sources in the same general region of the HDF.

bright star located in the HDF flanking fields. The observations were taken through a $1''.0$ wide slit oriented at $PA = 119^\circ.4$ to cover both the target object and a nearby star ($12''.8$ away) which served as a pointing reference. The target was dithered along the slit in an ABBA pattern using 100 second exposure times, and the count rate from the reference star was monitored to ensure that pointing remained stable. The target was periodically reacquired and placed at new positions along the slit. Seeing throughout all observations averaged $1''.0$. On 2 and 6 May we used grating 4 (200 lines/mm, blazed at $3\mu\text{m}$) at 1st order in the K -band ($\lambda\lambda 1.90\text{--}2.50\mu\text{m}$) giving an effective spectral resolution $R = \lambda/\Delta\lambda \approx 240$ at $\lambda 2.2\mu\text{m}$ as measured from night sky lines. On 3 and 6 May we also observed with grating 4 at 2nd order in the H -band ($\lambda\lambda 1.49\text{--}1.80\mu\text{m}$), with $R \approx 380$ at $\lambda 1.65\mu\text{m}$. The H -band data on 3 May were taken through occasional cirrus; frames with poor transparency (judged from the reference star) or bad sky subtraction were discarded from the analysis. The total exposure times retained for the final H and K -band grating 4 spectrograms were 13400s and 17600s, respectively. We reduced the data using standard procedures. The data were corrected for array non-linearity, and flat-fielded using dome flats. The sky was subtracted (to first order) using the ABBA differences. The wavelength scale and geometric distortion were calibrated using OH night sky lines, and the two dimensional spectral images were rectified. Residual sky features were then fit and subtracted. The images were positionally registered using the reference star, and combined using a bad pixel mask and a percentile-clipping scheme to reject outlying pixels. Spectra were extracted through a 3 pixel ($1''.05$) wide window at the nominal position of the object relative to the reference star, along with a noise measurement extracted from the 2-dimensional variance image created when the images were combined. Flux calibration was based on observations of the Elias *et al.* (1982) standard HD 105601, with absolute flux normalization based on the H and K_s magnitudes (measured from the IRIM HDF data) of the reference star on the slit.

The low-resolution H -band spectrogram (Figure 3) shows a possible emission line at $\lambda 1.643\mu\text{m}$, with flux $\approx 2 \times 10^{-16}$ erg s $^{-1}$ cm $^{-2}$ and integrated $S/N \approx 4.3$. Although the H -band sky is nearly covered with OH emission bands at this low dispersion, the telluric lines near this wavelength are relatively weak. We reobserved the object at higher spectral resolution ($R \approx 670$ at $\lambda 1.65\mu\text{m}$) on UT 1999 May 7 under good atmospheric conditions, using grating 1 (300 lines/mm, blazed at $4\mu\text{m}$) in 2nd order, covering $\lambda\lambda 1.51\text{--}1.69\mu\text{m}$. The putative emission line does not reproduce in the grating 1 spectrogram. The 3σ upper limit for an unresolved emission line at $1.643\mu\text{m}$ is $\approx 6 \times 10^{-17}$ erg s $^{-1}$ cm $^{-2}$.

Careful, frame-by-frame inspection of the grating 4 data does not reveal any obvious artifacts that could have produced the emission feature. It is present when the data are combined as a median (rather than percentile clipped averages), demonstrating that the feature results from systematically high data values and not from intermittent artifacts. We have tried to test its reality by subdividing the grating 4 exposures into independently averaged, randomly selected half data sets. However the S/N in each half-set is low; the apparent line sometimes appears in both, sometimes not. Its significance is hard to evaluate because noise in the data is correlated (e.g., sky

subtraction residuals) with greatly varying amplitude vs. wavelength. As a test, we normalized the coadded, two dimensional spectral image by the variance map to equalize the pixel-to-pixel RMS throughout, and extracted 26 spatially independent, 3 pixel wide spectra from regions of the slit unaffected by the reference star. Each extraction was subtracted to zero mean, and then convolved by a Gaussian with the instrumental resolution. We measured the peak value of the nominal emission line from JD1, and searched for features with equal or greater amplitude (positive or negative) at any wavelength in the other 25 “test” extractions. No comparable positive feature was found, and only one negative feature, suggesting a probability $\sim 2\%$ (1 out of 2×25) that the HDFN–JD1 “line” would arise by chance.

Our spectroscopic results are therefore ambiguous. The line in the grating 4 spectrogram is resilient but not ironclad. The fact that it does not reproduce in the grating 1 observation suggests either that it is not real, or that it is well resolved at the higher dispersion (thus reducing the detection sensitivity), or that the object was not well placed in the spectrograph slit on May 7.

The K –band spectrogram shows no significant emission features; the 3σ flux limit for an unresolved line ranges from 1 to 3×10^{-16} erg s $^{-1}$ cm $^{-2}$ over the range $\lambda\lambda 1.95\text{--}2.4\mu\text{m}$, and rises steeply at longer wavelengths due to the increasing thermal background. We would not have expected to (and did not) detect the object’s continuum at either K or H .

4. Angular Extent

The NICMOS F160W image of HDFN–JD1 is very compact, but there is evidence that it may be resolved. Examining ten well exposed, spectroscopically confirmed stars in our images, we measure the PSF FWHM to be $0''.217 \pm 0''.016$ ($0''.19$ to $0''.24$ maximum range), while JD1 has $\text{FWHM} = 0''.28$. Figure 4a compares the surface brightness profiles of the object and three faint, well isolated stars which have been registered and scaled using a non–negative cross–correlation procedure. The profile of HDFN–JD1 appears to be slightly more extended. Subtracting the scaled PSF stars from JD1 leaves positive annular residuals which are not present when one star is scaled and subtracted from another. Additionally, SExtractor computes a stellarity index using a neural network classifier which outputs values from 0 (extended) to 1 (stellar). The known HDF stars have stellarity ≥ 0.84 , while HDFN–JD1 has stellarity = 0.08 (Figure 4c). However, the object is near the faint limit where the classifier appears to be reliable. The NICMOS PSF may depend on source color, and HDFN–JD1 is extremely red while the stars are among the bluest objects in $J_{110} - H_{160}$. We have examined this using Tiny Tim models (Krist & Hook 1997) computed for a very wide range of source spectra and find it is too weak to account for the differences we measure. Proper analysis of the PSF from dithered images with NICMOS Camera 3 requires a realistic treatment of the known (and large) detector intrapixel sensitivity variations (cf. Lauer 1999). Therefore while our measurements suggest that the object is spatially extended, we cannot be completely confident about this given the present data. In the future, a robust angular extent measurement might be accomplished using NICMOS Camera 2, which critically samples the PSF

at $1.6\mu\text{m}$, when the instrument is resuscitated with the NICMOS Cooling System in HST Cycle 10.

Figure 5 compares the colors of HDFN–JD1 to those of a variety of cool or reddened stars. We have converted our NICMOS AB magnitudes to a conventional Vega scale for comparison to published stellar data, including an approximate color term to correct to standard J and H bandpasses. In this system, JD1 has $J - H \gtrsim 2.5$ (2σ) and $H - K \approx 1.6$. This is much redder than ordinary cool stars and known substellar objects, which can have extremely red optical-to-infrared colors but are generally rather blue in $J - H$ and $H - K$ where their spectra are dominated by strong molecular absorption. The reddest L dwarf stars reach $J - H = 1.45$, but the known “methane dwarfs” have $J - H \approx H - K \lesssim 0$. Atmosphere models (Burrows *et al.* 1997) predict still bluer colors for cooler brown dwarfs and giant extra-solar planets. The only known stars as red as HDFN–JD1 are those undergoing mass loss with thick circumstellar dust shells, such as extreme carbon stars or Mira variables. HDFN–JD1 is redder than ordinary galactic or Magellanic AGB stars, but the most heavily reddened objects like IRC +10216 and some extreme Miras can equal or exceed its colors.⁹ It would be remarkable to encounter such an unusual star in a tiny, high galactic latitude field such as the HDF. Moreover, at K it is 11.9 magnitudes fainter than the reddest LMC carbon stars, implying (by analogy) a distance ~ 12 Mpc. A blackbody with $T \approx 1050\text{K}$ also matches the $H_{160} - K_s$ color and 2σ $J_{110} - H_{160}$ limit for HDFN–JD1 quite well, but no known star has such a spectrum. Recent atmosphere models for cool white dwarfs (e.g., Hansen 1998; Saumon & Jacobson 1999) suggest that they should have very blue colors due to H_2 opacity.

5. Discussion

The salient photometric features HDFN–JD1 are firm detections at H_{160} and K_s , and very faint upper limits (possibly with some $S/N \lesssim 2$ detections) at all shorter wavelengths. The bandpass-averaged f_ν flux density declines by a factor of 3.1 from $2.2\mu\text{m}$ to $1.6\mu\text{m}$, and then again from $1.6\mu\text{m}$ to $1.1\mu\text{m}$ by a factor $34_{-21}^{+\infty}$ (1σ errors), with a 97.7% (1-sided) confidence limit > 8.3 , implying curvature or a break in the spectral energy distribution. This is the only object in the NICMOS HDF–N at $H_{160} < 26$ which is undetected (with $S/N < 2$) in any of the optical WFPC2 bandpasses. It is by far the reddest HDF–N object in $J_{110} - H_{160}$, but also one of the reddest in $H_{160} - K_s$. Only one (slightly) brighter HDF object, a $z = 3.2$ “ U -dropout” galaxy, has a redder $H_{160} - K_s$ color (but equal within the 1σ measurement uncertainties). That galaxy’s color probably results from a strong Balmer and/or 4000\AA break, or possibly from strong [OIII]+H β line emission in the K_s band.

⁹IRC +10216 itself, scaled to the H_{160} or K_s magnitude of HDFN–JD1, should have been detected in the ISO images of the HDF at 7 and $15\mu\text{m}$.

There are three common reasons why a galaxy’s spectral energy distribution (SED) may appear to be very red: extinction, age, or the presence of a strong spectral break, such as that caused by the Lyman limit or Lyman α forest. Here we consider each of these in turn, making comparisons wherever possible to photometry of actual galaxies from the HDF and elsewhere in order to avoid overreliance on models. One way of comparing colors in different bandpass combinations is to parameterize the photometry by a spectral index α , i.e. $f_\nu \propto \nu^{-\alpha}$. For two bandpasses with effective wavelengths λ_1 and λ_2 and magnitude measurements m_1 and m_2 , we may define $\alpha_{(m_1-m_2)} = 0.4(m_1 - m_2)/\log(\lambda_2/\lambda_1)$. The nominal HDFN–JD1 $J_{110} - H_{160}$ color corresponds to $\alpha_{(J-H)} = 10.2$, and the 1σ and 2σ limits to $\alpha_{(J-H)} > 7.5$ and > 6.1 , respectively. Considering pairs of adjacent HDF bandpasses U_{300} through J_{110} , we find a few other galaxies with comparably steep spectra at shorter wavelengths. Among these, the objects with spectroscopic identifications are invariably either Lyman break “dropouts” or red, early–type galaxies, and the as–yet unidentified objects all appear to be consistent with being members of one of these two classes.

Dust may, in principle, redden a spectrum almost arbitrarily. Because extinction laws generally steepen in the UV, a red and possibly strongly curved SED may result when the UV portion of a distant, dusty galaxy redshifts into optical or near–IR bandpasses. One well–known and fairly extreme example is the object discovered by Hu & Ridgway (1994) and colloquially known as HR10, with $z = 1.44$ (Graham & Dey 1996). Sub–mm measurements by Cimatti *et al.* (1998) and Dey *et al.* (1999) have shown that it is probably a dust–enshrouded, star forming galaxy or AGN. The SED of HR10 is steepest between I and J (Dey *et al.* 1999), with $\alpha_{(I-J)} = 6.1$. An object like HR10 shifted to $z \approx 2.3$ would have colors roughly consistent with our measured 2σ limits on HDFN–JD1 (see Figure 6). A somewhat redder SED might be needed to fully match the photometry of JD1, but this could presumably be accomplished by adding still more dust. HR10 is compact in Keck K –band images, but diffuse ($\approx 1''.2$ in size) and bimodal in WFPC2 images which sample the rest–frame UV light (Dey *et al.* 1999). Similar changes in morphology with wavelength could make it difficult to detect a fainter, more distant analog to HR10 in the WFPC2 HDF. Adopting (here and below) a cosmology with $\Omega_M = 0.3$, $\Omega_\Lambda = 0.7$, and $H_0 = 70 \text{ km s}^{-1} \text{ Mpc}^{-1}$, HDFN–JD1 at $z \approx 2.3$ would have a rest–frame B –band luminosity $\approx 0.12\times$ that of HR10. Scaling the far–IR emission from HR10 accordingly, the predicted $850\mu\text{m}$ flux would be $\sim 0.5 \text{ mJy}$, or a factor of four below the current SCUBA limits for the HDF. Objects as red as HR10 are relatively rare, and it may seem surprising to find an even redder example within the 5 arcmin^2 of the HDF, but little is known about their numbers at these faint magnitudes. The fact that there are only a handful of objects with such extreme IR colors in the HDF suggests that they are not a common population by number relative to ordinary, relatively unreddened galaxies, but their unobscured luminosities and star formation rates might be quite large and important in the scheme of galaxy formation. Some of the faint sub–mm sources detected in recent surveys are red objects like HR10 (e.g., Smail *et al.* 1999), although it is worth noting that none of the candidate counterparts to sub–mm sources in the HDF has particularly unusual colors (Dickinson *et al.*, in preparation).

The integrated spectrum of an old stellar population is steepest in the near ultraviolet, from the familiar 4000Å break through spectral breaks at 2900Å, and 2640Å (Morton *et al.* 1977). At $2.5 \lesssim z \lesssim 4.5$ these breaks would redshift beyond the WFPC2 bandpasses into the near-IR, maximizing the $J_{110} - H_{160}$ color. The resulting k -correction could make old, high redshift ellipticals nearly invisible in the optical HDF (e.g., Maoz 1997). For example, the observed-frame colors of the giant elliptical galaxy HDF 4-752.1 at $z = 1.013$ correspond to $\alpha_{(B-V)} \approx 10.2$ and $\alpha_{(V-I)} \approx 6.3$. Shifted to $z \gtrsim 3$, its SED would roughly match that of HDFN-JD1 (Figure 6). However, this would require that a $z \approx 3$ elliptical have a spectrum nearly as red as that of 4-752.1 at $z = 1$, despite the universe being considerably younger. This is difficult to explain without invoking an unusual IMF, an unpopular cosmology, or extinction. Figure 7 shows the infrared colors of HDF galaxies with known redshifts, along with models computed using the population synthesis code of Bruzual & Charlot (1993, 1996). The reddest model traces a solar metallicity population formed with a Salpeter IMF in a short burst at $z = 15$ and aging passively thereafter. The $H_{160} - K_s$ color of HDFN-JD1 is reasonably matched for $3 < z < 6$, but the $J_{110} - H_{160}$ color of the model does not quite reach the formal 2σ color limit for JD1 at any redshift. At $z = 3.5$ in our adopted cosmology, HDFN-JD1 would have an absolute B magnitude $M_B \approx -21.6$. If it were an “old” elliptical galaxy at $z \gtrsim 3$, this would strongly suggest that at least some galaxies formed the bulk of their stars at extremely large redshifts. If so, however, then it is puzzling that there are no other HDF galaxies nearly as red, as might be expected if there were a continuum of such objects extending out to $z \approx 3$. Red, early-type galaxies have been identified spectroscopically out to $z = 1.55$ (e.g., Dunlop *et al.* 1996; Spinrad *et al.* 1997; Dickinson 1997; Dey 1998) and photometrically in the HDF and elsewhere out to $z \approx 2$ (cf. Stiavelli *et al.* 1999, Benítez *et al.* 1999), but HDFN-JD1 would stand alone as a unique example at significantly larger redshift.

The Lyman limit can effectively truncate the spectrum of high redshift objects, making them appear arbitrarily red in certain color combinations. The $z > 5$ “V-dropout” galaxies HDF 4-473 and 3-951 (Weymann *et al.* 1998, Spinrad *et al.* 1998) and the $z = 4.022$ “B-dropout” HDF 3-512 (Dickinson 1998) all have $\alpha > 7.3$ for colors that span the Lyman limit, and several $z \sim 3$ “U-dropouts” have $\alpha_{(U-B)} > 6$. At $z \gtrsim 3$, an additional break is introduced by the Lyman α forest, which is increasingly thick at higher redshifts and affects broad band colors to a correspondingly greater degree (cf. Lowenthal *et al.* 1997, Dickinson 1998). We do not know the opacity of the Lyman α forest at $z > 6$, but may reasonably assume that it continues to increase since we believe that the universe was dominated by neutral hydrogen beyond some reionization redshift.

If we interpret HDFN-JD1 as a Lyman break object, then its $J_{110} - H_{160}$ color is matched for $z \gtrsim 10$, but the red $H_{160} - K_s$ color suggests that the Lyman α forest has eaten away roughly half of the H_{160} flux, implying a redshift $z \approx 12.5$ (see Figure 7). At that redshift, the K -band corresponds to $\lambda_0 = 1600\text{Å}$ in the emitted frame, essentially the same wavelength where Steidel *et al.* select galaxies in their survey at $z \approx 3$. We may therefore make a direct comparison to the observed $z \approx 3$ luminosity function (Dickinson 1998, Steidel *et al.* 1999). For an $\Omega_M = 0.3$,

$\Omega_\Lambda = 0.7$ cosmology, HDFN–JD1 would be $\approx 3\times$ more luminous than the brightest Lyman break galaxy from our 0.3 deg^2 ground–based survey. This may seem improbable, given the small solid angle of the HDF. However, the total co–moving HDF volume out to $z = 12.5$ is quite large, particularly for an open or Λ –dominated cosmology. For $\Omega_M = 0.3$, $\Omega_\Lambda = 0.7$, it is equivalent to the effective volume of the U_nGR Lyman break selection function (see Steidel *et al.* 1999) over a 100 arcmin^2 field. Because the volume is heavily weighted toward the highest redshifts, then it is not unlikely that the rarest, most luminous objects would also be the most distant, provided that they exist at all beyond $z > 6$. In our ground–based survey we often find $z \approx 3$ QSOs that are brighter than the most luminous Lyman break galaxies, and the nearly unresolved morphology of HDFN–JD1 might plausibly indicate that it is some sort of AGN. Populations of distant QSOs have been postulated as a means of reionizing the universe at high redshift, although existing models for the formation of high redshift AGN (Haiman & Loeb 1998; Haehnelt, Natarajan, & Rees 1998) would predict that no objects as bright as HDFN–JD1 should be found within the HDF volume at $z > 10$.

If HDFN–JD1 were a galaxy forming stars at $z = 12.5$ with a Salpeter IMF and without dust, its UV luminosity would correspond to a star formation rate $\approx 180h_{70}^{-2} M_\odot/\text{yr}$ (70 or $400h_{70}^{-2} M_\odot/\text{yr}$ for Einstein–de Sitter or $\Omega_M = 0.2$ open universes). This is the sort of rate required by monolithic collapse models which would form a $10^{11} M_\odot$ galaxy within a short ($\lesssim 10^9 \text{ yr}$) time scale, and is also comparable to the *obscured* star formation rates which have been claimed for high redshift sub–mm sources. However, if HDFN–JD1 resembles a classical, unobscured protogalaxy, then such objects are evidently quite rare. We will present a more complete discussion of color–selected high redshift galaxy candidates from our NICMOS survey in a future paper, but there are no U , B , V or I “dropout” candidates in the HDF with luminosities comparable to that which HDFN–JD1 would have if it were at $z = 12.5$. One such object in the redshift range $2 < z < 12.5$ implies a space density $\sim 10^{-5} h_{70}^3 \text{ Mpc}^{-3}$ for our assumed cosmology, and $4.3\times$ larger for an Einstein–de Sitter universe. This is a few hundred times smaller than the present–day space density of $\sim L^*$ galaxies ($\phi^* = 4 \text{ to } 6h_{70}^3 \times 10^{-3} \text{ Mpc}^{-3}$ from the K –band luminosity functions of Gardner *et al.* 1997, Szokoly *et al.* 1998, Mobasher *et al.* 1993, and Loveday 1999). If rapid, monolithic galaxy formation took place anywhere in that redshift range, then either it was quite uncommon, or it was obscured by dust. Lanzetta *et al.* (1998) reached very similar conclusions based on their search for optically invisible objects in the KPNO infrared HDF data. If perhaps only the rarest, most massive galaxies, e.g., brightest cluster ellipticals (BCEs), formed their stars rapidly at the highest redshifts, then HDFN–JD1 could be one example. The present–day space density of galaxy clusters with Abell richness class ≥ 1 or X–ray temperature $kT \geq 2.5 \text{ keV}$ is $\approx 3 \times 10^{-6} h_{70}^3 \text{ Mpc}^{-3}$ (cf. Eke, Cole, & Frenk 1996), implying that we might expect $\sim 1/3$ “proto–BCEs” per HDF volume.

From Figures 7 and 1 it is evident that a star–forming galaxy at $z \gtrsim 9.5$ should have $J_{110} - H_{160} \gtrsim 1.5$ due to the Lyman limit, and also that HDFN–JD1 is the only such object in the HDF–N with $H_{160} < 26$, the magnitude down to which we could measure such a color or

limit with $> 2\sigma$ significance.¹⁰ There are, therefore, no other *detected* candidates for galaxies at $z > 9.5$ in the HDF, although cosmological surface brightness dimming could significantly affect sensitivity to extended protogalaxies at such redshifts, even in deep images such as these. At $z = 9.5$, the $H_{160} = 26$ limit corresponds to an unobscured star formation rate $\approx 20h_{70}^{-2} M_{\odot} \text{ yr}^{-1}$ for our adopted cosmology.

The possible $1.643\mu\text{m}$ emission line seen in the CRSP spectra could be consistent with any of these interpretations. For a dusty galaxy or AGN, it might be [OIII] $\lambda 5007\text{\AA}$ at $z = 2.28$. $\text{H}\alpha$ at $z \approx 1.5$ is also possible, but it is much easier to match the colors at $z \gtrsim 2$ where the J_{110} band would sample the rest-frame UV. Alternatively the line could be [OII] $\lambda 3727\text{\AA}$ at $z = 3.40$, a redshift where an old stellar population nearly matches the colors of HDFN–JD1. An emission line, however, might suggest active star formation inconsistent with a maximally old elliptical galaxy, thus requiring either the presence of an AGN, dust, or both. A reddened, star forming object at this redshift is also possible. Finally, the line could be Lyman α at $z = 12.51$, where the JHK colors are well matched by the Lyman break hypothesis. However, given the fact that the line did not reproduce in our reobservation (see §3 above), we cannot be confident that it was real and do not further consider the spectroscopic possibilities here.

An alternative explanation for the peculiar colors would be the presence of very strong line emission in one or more infrared bands. Line fluxes ~ 1.5 and $2 \times 10^{-16} \text{ erg s}^{-1} \text{ cm}^{-2}$ in the H_{160} and K_s bands, respectively, could mimic the broad band fluxes measured for HDFN–JD1. The possible $1.643\mu\text{m}$ emission line, if real, could therefore account for the entire signal detected in the NICMOS H_{160} image. Detection at both H_{160} and K_s makes the “pure emission line” hypothesis seem less plausible, however, requiring either strong lines in both bands or an extremely red continuum. In the latter case, we are forced back to our previous speculations.

6. Conclusion

Without further data, we cannot unambiguously distinguish between these explanations for the nature of HDFN–JD1. Each, however, is quite remarkable in its own right. Perhaps the least “exotic” extragalactic hypothesis is that HDFN–JD1 is a dusty, HR10–like galaxy at $z \gtrsim 2$. Such objects, with sub-mm fluxes just below the current SCUBA detection limits, might be sufficiently common to make up the bulk of the far-infrared background (Barger, Cowie & Sanders 1999). The possibility that HDFN–JD1 is an “old” elliptical galaxy at $z \gtrsim 3$ is perhaps more remarkable, in that it would strongly suggest that at least some galaxies formed the bulk of their stars at very large redshifts.¹¹

¹⁰The radio source counterpart J123651.7+621221.4 is well detected in the B_{450} , V_{606} and I_{814} optical passbands, and thus is not at $z \gg 3$.

¹¹When first forming stars, the $z > 10$ progenitor to an old, $z \approx 3.5$ elliptical might well resemble HDFN–JD1.

Perhaps the most spectacular interpretation of this object, but also the one requiring the most rigorous proof, would be that it lies at $z > 10$, an extremely distant analog of the Lyman break galaxy population. If this were the case, then its high luminosity and the relatively small volume of the HDF would suggest that we were either extremely lucky, or that such objects were more common than would be expected based on an extrapolation of the $z \approx 3$ population to higher redshifts. If the luminosity results from star formation, then HDFN–JD1 would resemble the classical picture of a protogalaxy, forming stars at $\gtrsim 100M_{\odot}/\text{yr}$. However, the implied space density of *unobscured* objects with such star formation rates is far smaller than that of L^* galaxies today. If galaxies formed monolithically at high redshift, then this was either a rare occurrence, or the process was largely enshrouded by dust, as has been suggested by the recent detection of distant sub–mm sources. If, instead, HDFN–JD1 were a QSO, it could be part of the population of objects responsible for re–ionizing the universe. From our NICMOS HDF data, we should be able to identify unreddened, compact objects with star formation rates $\sim 20h_{70}^{-2}M_{\odot}/\text{yr}$ at $z \approx 9.5$, with the limit rising to $\sim 100h_{70}^{-2}M_{\odot}/\text{yr}$ at $z = 13$ as the Lyman α forest suppresses the H_{160} flux. No candidates other than HDFN–JD1 are seen.

Distinguishing between the possible explanations for this object will require new observations, but none will be easy. Spectroscopy will be challenging even with the new generation of IR instruments on 8 to 10m telescopes, and there is no guarantee that the object has detectable emission lines. Although our understanding of the transparency of the IGM at $z > 5$ is based solely on extrapolation, a robust optical detection would probably exclude the Lyman break hypothesis. Occasionally, QSO sightlines at lower redshifts are free of optically thick H I absorption (e.g., Reimers *et al.* 1992), but it seems unlikely that emitted–frame Lyman continuum from an ordinary galaxy or QSO could propagate through the universe from $z \approx 12$ without being absorbed. The optical measurement in §2 is suggestive but not highly significant; a deeper optical image, e.g., with STIS or the forthcoming HST Advanced Camera for Surveys, would be a valuable (albeit expensive) observation. Photometry at $\lambda \gtrsim 3\mu\text{m}$ with IRAC on SIRTf could distinguish between the $z > 10$ Lyman break and $z < 6$ red galaxy hypotheses, since the spectra of red galaxies should continue to rise toward longer wavelengths, with $f_{\nu} \gtrsim 2\mu\text{Jy}$, while a star forming galaxy at $z > 10$ should have a flatter, fainter SED (see Figure 6). If near–IR spectroscopy fails to detect emission lines, then the best hopes for distinguishing between the old galaxy and reddened starburst/AGN models lie at longer wavelengths. Given that the HDF already has the deepest (and possibly confusion limited) SCUBA observation, a true sub–mm detection may require a future generation of telescopes and instruments. A detection would certainly imply dust, but given the negative sub–mm k –correction it probably would not distinguish between “low” ($z \sim 2$) and high ($z \sim 12$) redshifts without multifrequency measurements. For a reddened starburst at $z \sim 2.3$, the dust emission should peak near $\sim 200\mu\text{m}$ and might be detectable by the SIRTf MIPS instrument near its confusion limit. SIRTf IRAC photometry from 3.6 to $8\mu\text{m}$ may prove useful, although disentangling reddening and age from broad band SEDs is notoriously difficult.

Regardless of its nature, the fact that such an unusual and extreme object was found in

a 5 arcmin² field suggests that there are interesting surprises awaiting future, wide-field, deep infrared surveys.

We would like to thank the other members of our HDF–N/NICMOS GO team who have contributed to many aspects of this program, and the STScI staff who helped to ensure that the observations were carried out in an optimal manner. We also thank the support staff at KPNO and the W.M. Keck Observatories for their help in carrying out the ground-based observations, especially Dick Joyce for verifying the CRSP plate scale. We thank Ron Gilliland for providing his additional WFPC2 images of the HDF, Eric Richards for digital VLA maps, and Sandy Leggett for digital tables of stellar photometry. Arjun Dey and the editor, Greg Bothun, carefully read the manuscript and made helpful suggestions. Jim Liebert, Michael Liu and William Bidelman provided guidance and references concerning colors of unusual galactic stars. Support for this work was provided by NASA through grant number GO-07817.01-96A from the Space Telescope Science Institute, which is operated by the Association of Universities for Research in Astronomy, Inc., under NASA contract NAS5-26555.

REFERENCES

- Aussel, H., Cesarsky, C.J., Elbaz, D., & Starck, J.L. 1999, *A&A*, 342, 313
- Barger, A.J., Cowie, L.L., & Sanders, D.B., 1999, *ApJ*, in press
- Becklin, E.E., Frogel, J.A., Hyland, A.R., Kristian, J., & Neugebauer, G. 1969, *ApJ*, 158, L133
- Benítez, N., Broadhurst, T., Bouwens, R., Silk, J., & Rosati, P. 1999, *ApJ*, 515, L65
- Bertin, E., & Arnouts, S. 1996, *A&AS*, 117, 393
- Brunner, R.J., Connolly, A.J., & Szalay, A.S. 1999, *ApJ*, 516, 563.
- Bruzual, G., & Charlot, S. 1993, *ApJ*, 405, 538
- Bruzual, G., & Charlot, S. 1996, personal communication
- Burgasser, A.J., *et al.* 1999, *ApJ*, in press
- Burrows, A., *et al.* 1997, *ApJ*, 491, 856
- Cimatti, A., Andreani, P., Rottgering, H., & Tilanus, R. 1998, *Nature*, 392, 895
- Cohen, J.G., Cowie, L.L., Hogg, D.W., Songaila, A., Blandford, R., Hu, E.M., & Shopbell, P. 1996, *ApJ*, 471, L5
- Costa, E., & Frogel, J.A. 1996, *AJ*, 112, 2607
- Désert, F.-X., Puget, J.-L., Clements, D.L., Péroult, M., Abergel, A., Bernard, J.-P., & Cesarsky, C.J. 1999, *A&A*, 342, 363
- Dey, A, Graham, J.R., Ivison, R.J., Smail, I., Wright, G.S., & Liu, M.C. 1999, *ApJ*, in press
- Dey, A. 1998, in *The Most Distant Radio Galaxies*, proceedings of the 1997 KNAW colloquium, astro-ph/9802163
- Dickinson, M. 1997, in *Galaxy Scaling Relations*, eds. L.N. da Costa & A. Renzini, (Berlin: Springer), p. 215
- Dickinson, M. 1998, in *The Hubble Deep Field*, eds. M. Livio, S.M. Fall & P. Madau, (Cambridge: Cambridge University Press), p. 219
- Downes, D., *et al.* 1999, *A&A*, in press
- Dunlop, J., Peacock, J., Spinrad, H., Dey, A., Jiminez, R., Stern, D., & Windhorst, R. 1996, *Nature*, 381, 581
- Eke, V.R., Cole, S., & Frenk, C.S. 1996, *MNRAS*, 282, 263
- Elias, J.H., Frogel, J.A., Matthews, K., & Neugebauer, G. 1982, *AJ*, 87, 1029
- Elston, R., Rieke, G.H., & Rieke, M.J. 1998, *ApJ*, 331, L77
- Elston, R., Rieke, M.J., & Rieke, G.H. 1999, *ApJ*, 341, 80
- Fernández-Soto, A., Lanzetta, K.M., & Yahil, A. 1999, *ApJ*, 513, 34
- Frogel, J.A., Mould, J., & Blanco, V.M. 1990, *ApJ*, 352, 96

- Frogel, J.A., Terndrup, D.M., Blanco, V.M., & Whitford, A.E. 1990, *ApJ*, 353, 494
- Fruchter, A.S., and Hook, R.N. 1999, *PASP*, submitted
- Gardner, J.P., Sharples, R.M., Frenk, C.S., & Carrasco, B.E. 1997, *ApJ*, 480, L99
- Gilliland, R.L., Nugent, P.E., & Phillips, M.M. 1999, *ApJ*, in press
- Goldschmidt, P., *et al.* 1997, *MNRAS*, 289, 465
- Graham, J.R., & Dey, A. 1996, *ApJ*, 471, 720
- Guhathakurta, P., Tyson, J.A., & Majewski, S.R. 1990, *ApJ*, 357, L9
- Haehnelt, M.G., Natarajan, P., & Rees, M.J. 1998, *MNRAS*, 300, 817
- Haiman, Z., & Loeb, A. 1998, *ApJ*, 503, 505
- Hansen, B.M.S. 1998, *Nature*, 394, 860
- Harris, H.C., Dahn, C.C., Vrba, F.J., Harden, A.A., Liebert, J., Schmidt, G.D., & Reid, I.N. 1999, *ApJ*, in press
- Hu, E.M., & Ridgway, S.E. 1994, *AJ*, 107, 1303
- Hughes, D., *et al.* 1998, *Nature*, 394, 241
- Joyce, D. 1995, *Cryogenic Spectrograph User's Manual*, (Tucson: NOAO)
- Kirkpatrick, *et al.* 1999, *ApJ*, 519, 802
- Krist, J., & Hook, R. 1997, *The Tiny Tim User's Guide* (version 4.4), (Baltimore: STScI)
- Lanzetta, K.M., Yahil, A., & Fernández-Soto, A. 1996, *Nature*, 381, 759
- Lanzetta, K.M., Yahil, A., & Fernández-Soto, A. 1998, *AJ*, 116, 1066
- Lauer, T.R. 1999, *PASP*, submitted
- Leggett, S.K. 1992, *ApJS*, 82, 351
- Leggett, S.K., Allard, F., & Hauschildt, P.H. 1998, *ApJ*, 509, 836
- Leggett, S.K., Toomey, D.W., Geballe, T.R., & Brown, R.H. 1999, *ApJ*, 517, L139
- Loveday, J., 1999, *MNRAS*, in press
- Lowenthal, J.D., *et al.* 1997, *ApJ*, 481, 673
- Madau, P. 1995, *ApJ*, 441, 18
- Maoz, D. 1997, *ApJ*, 490, L135
- Matthews, K.Y., & Soifer, B.T. 1994, in *IR Astronomy With Arrays*, ed. I. McLean, (Dordrecht: Kluwer), 239
- Mobasher, B., Sharples, R.M., & Ellis, R. 1993, *MNRAS*, 263, 560
- Morton, D.C., Spinrad, H., Bruzual, G., & Kurucz, R.L. 1977, *ApJ*, 212, 438
- Oestreich, M.O., Schmidt-Kaler, Th., & Wargau, W. 1997, *MNRAS*, 289, 729

- Reimers, D., Vogel, S., Hagen, H.-J., Engels, D., Groot, D., Wamsteker, W., Clavel, J., & Rosa, M.R. 1992, *Nature*, 360, 561
- Richards, E.A., Kellerman, K.I., Fomalont, E.B., Windhorst, R.A., & Partridge, R.B. 1998, *AJ*, 116, 1039
- Richards, E.A. 1999, *ApJ*, 513, L9.
- Saumon, D., & Jacobson, S.B. 1999, *ApJ*, 511, L107
- Skinner, C.J., *et al.* 1998, *SPIE*, 3354, 2
- Smail, I., Ivison, R.J., Kneib, J.-P., Cowie, L.L., Blain, A.W., Barger, A.J., Owen, F.N., & Morrison, G.E. 1999, *MNRAS*, in press
- Spinrad, H., Dey, A., Stern, D., Dunlop, J., Peacock, J., Jimenez, R., & Windhorst, R. 1997, *ApJ*, 484, 581
- Spinrad, H., Stern, D., Bunker, A., Dey, A., Lanzetta, K.M., Yahil, A., Pascarelle, S., & Fernández-Soto, A. 1998, *AJ*, 116, 2617
- Steidel, C.C., Giavalisco, M., Pettini, M., Dickinson, M., & Adelberger, K.L. 1996a, *ApJ*, 462, L17
- Steidel, C.C., Giavalisco, M., Dickinson, M., & Adelberger, K.L. 1996b, *AJ*, 112, 352
- Steidel, C.C., Adelberger, K.L., Giavalisco, M., Dickinson, M., & Pettini, M. 1999, *ApJ*, 519, 1
- Stiavelli, M., *et al.* 1999, *A&A*, 343, L25
- Strauss, M., *et al.* 1999, *ApJ*, submitted
- Szalay, A.S., Connolly, A.J., & Szokoly, G.P. 1999, *AJ*, 117, 68
- Szokoly, G.P., Subbarao, M.U., Connolly, A.J., & Mobasher, B. 1998, *ApJ*, 492, 452
- Thompson, D., *et al.* 1999, *ApJ*, in press
- Thompson, R.I., Rieke, M., Schneider, G., Hines, D.C., & Corbin, M.R. 1998, *ApJ*, 492, L95
- Veron, P. 1983, in *Quasars and Gravitational Lenses*, Université de Liège, Institute d’Astrophysique, p. 210
- Waddington, I., Windhorst, R. A., Cohen, S. H., Partridge, R. B., Spinrad, H., & Stern, D. 1999, *ApJL*, submitted
- Warren, S.J., Hewitt, P.C., Irwin, M.J., McMahon, R.G., Bridgeland, M.T., Bunclark, P.S., & Kibblewhite, E.J. 1987, *Nature*, 325, 131
- Weymann, R.J., Stern, D., Bunker, A., Spinrad, H., Chaffee, F.H., Thompson, R.I., & Storrie-Lombardi, L.J. 1998, *ApJ*, 505, L95
- Whitelock, P., Menzies, J., Feast, M., Marang, F., Carter, B., Roberts, G., Catchpole, R., & Chapman, J. 1994, *MNRAS*, 267, 711
- Whitelock, P., Menzies, J., Feast, M., Catchpole, R., Marang, F., & Carter, B. 1995, *MNRAS*, 276, 219

Williams, R.E., *et al.* 1996, AJ, 112, 1335

Williams, R.E., *et al.* 1999, in preparation

Table 1. Photometry of J123656.3+621322

Instrument	Bandpass	Wavelength	Flux Density ^a	AB Magnitude ^b
NIRC	K_s	$2.16\mu\text{m}$	995.0 ± 182.5 nJy	$23.91^{+0.22}_{-0.18}$
NICMOS	H_{160}	$1.61\mu\text{m}$	318.1 ± 13.8 nJy	$25.14^{+0.05}_{-0.05}$
NICMOS	J_{110}	$1.14\mu\text{m}$	9.3 ± 14.6 nJy	> 27.44
WFPC2	I_{814}	$0.80\mu\text{m}$	6.1 ± 4.1 nJy	> 28.51
WFPC2	V_{606}	$0.60\mu\text{m}$	4.3 ± 2.4 nJy	> 29.00
WFPC2	B_{450}	$0.46\mu\text{m}$	1.5 ± 3.6 nJy	> 29.05
WFPC2	U_{300}	$0.30\mu\text{m}$	-2.5 ± 7.5 nJy	> 28.66

^aFluxes and uncertainties with aperture corrections to “total” values (see text).

^bWhen $S/N < 2$, magnitudes are quoted as 2σ limits.

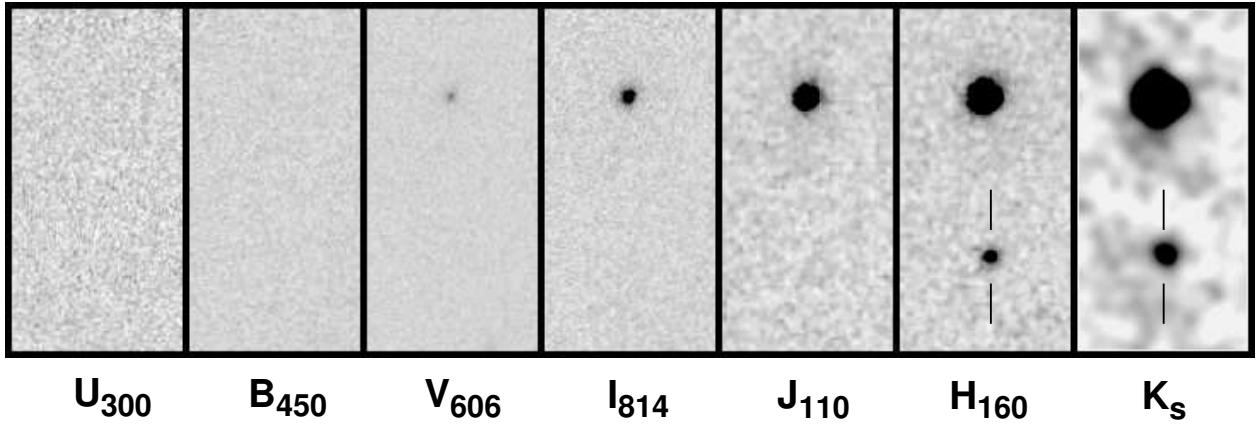


Fig. 1.— HST and Keck images of HDFN–JD1 at $0.3\text{--}2.16\mu\text{m}$. The field of view of each panel is $4'' \times 8''$, and north is $23^\circ.8$ counterclockwise from vertical. HDFN–JD1 is identified by tick marks in the H_{160} and K_s panels, and is located at J2000 coordinates $\alpha = 12:36:56.32$, $\delta = 62:13:21.7$. The NIRC K_s image has been smoothed by a Gaussian with $\text{FWHM} = 0''.38$. A constant grey level corresponds to constant f_ν surface brightness. The elliptical galaxy at top (HDF 3-48.0) is very red in its own right; its estimated photometric redshift is $z \approx 1.25$ (Budavari *et al.*, in preparation).

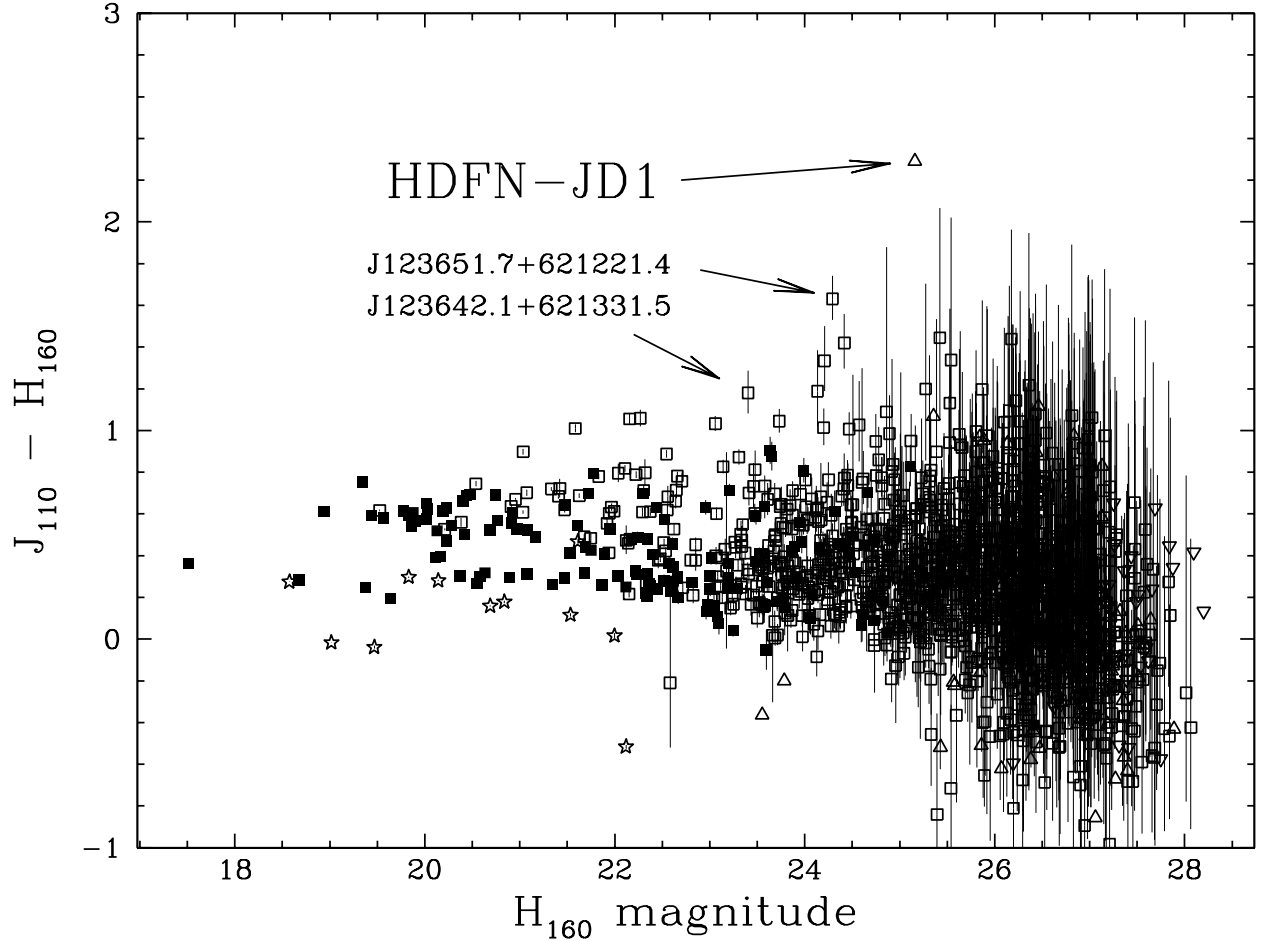


Fig. 2.— $J_{110} - H_{160}$ versus H_{160} color-magnitude diagram (on the AB system) for the HDF-N NICMOS-selected catalog. Filled and open squares indicate galaxies with and without spectroscopic redshifts, respectively, while known stars are marked by star symbols. Colors are plotted with $\pm 1\sigma$ error bars, and measurements with $S/N < 2$ are marked by triangles at the 2σ color limit. HDFN-JD1 is labeled; its 1σ color limit would be $J_{110} - H_{160} > 2.8$. The next-reddest galaxy, J123651.7+621221.4, is a faint cm radio source. Another VLA source, J123642.1+621331.5, is also unusually red (Richards *et al.* 1998, Waddington *et al.* 1999, submitted).

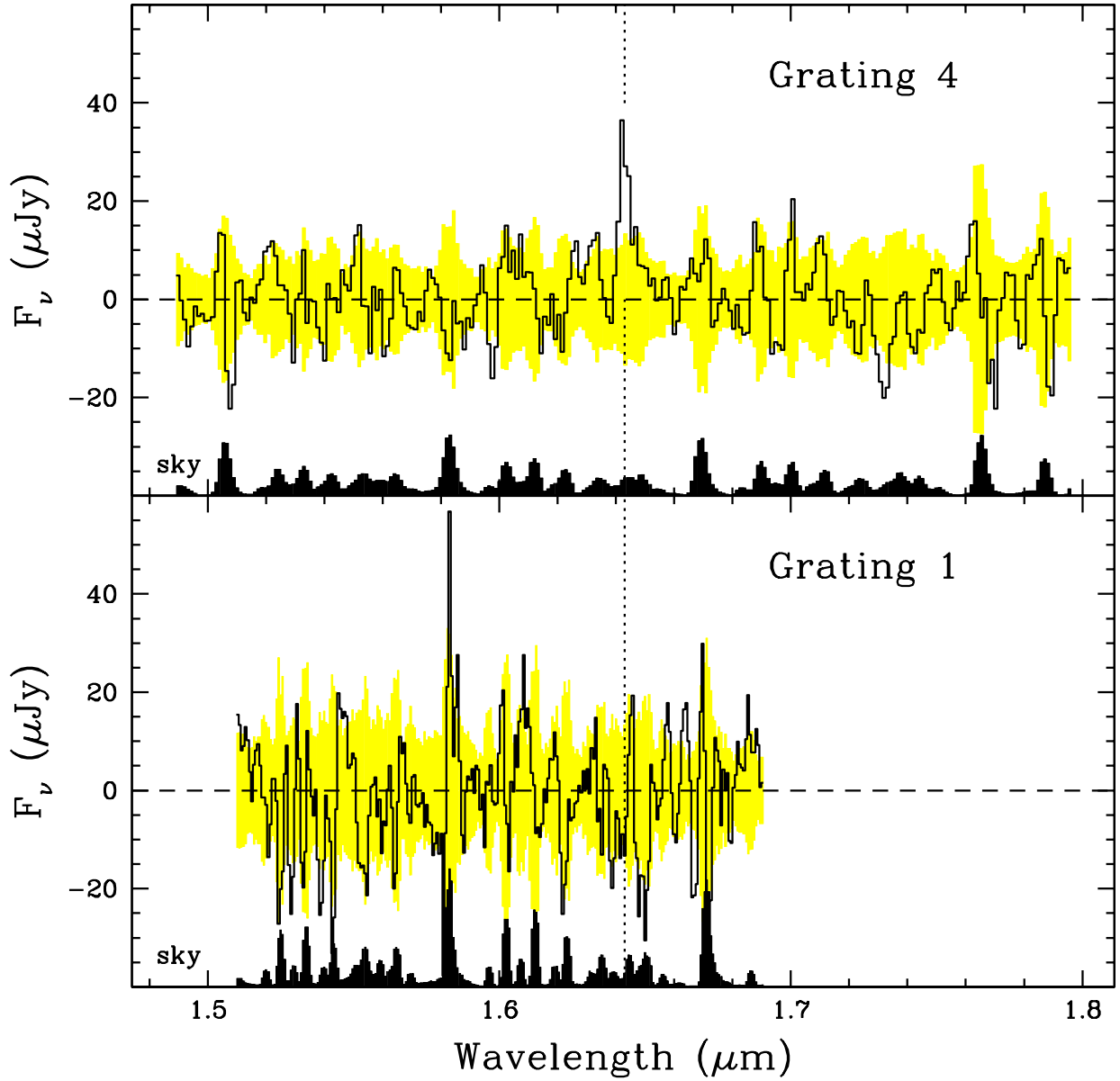


Fig. 3.— H -band spectrograms of HDFN-JD1 obtained with CRSP at the KPNO 4m. The spectra have been smoothed by a 3-pixel boxcar. The lightly shaded regions show the $\pm 1\sigma$ noise level of the data (before smoothing), and greatly suppressed sky spectra are plotted along the bottom axis. The low-resolution grating 4 spectrogram (top) shows a possible emission line at $\lambda 1.643\mu\text{m}$, but this is not detected in the subsequent, higher resolution grating 1 spectrogram (bottom), leaving its reality in doubt.

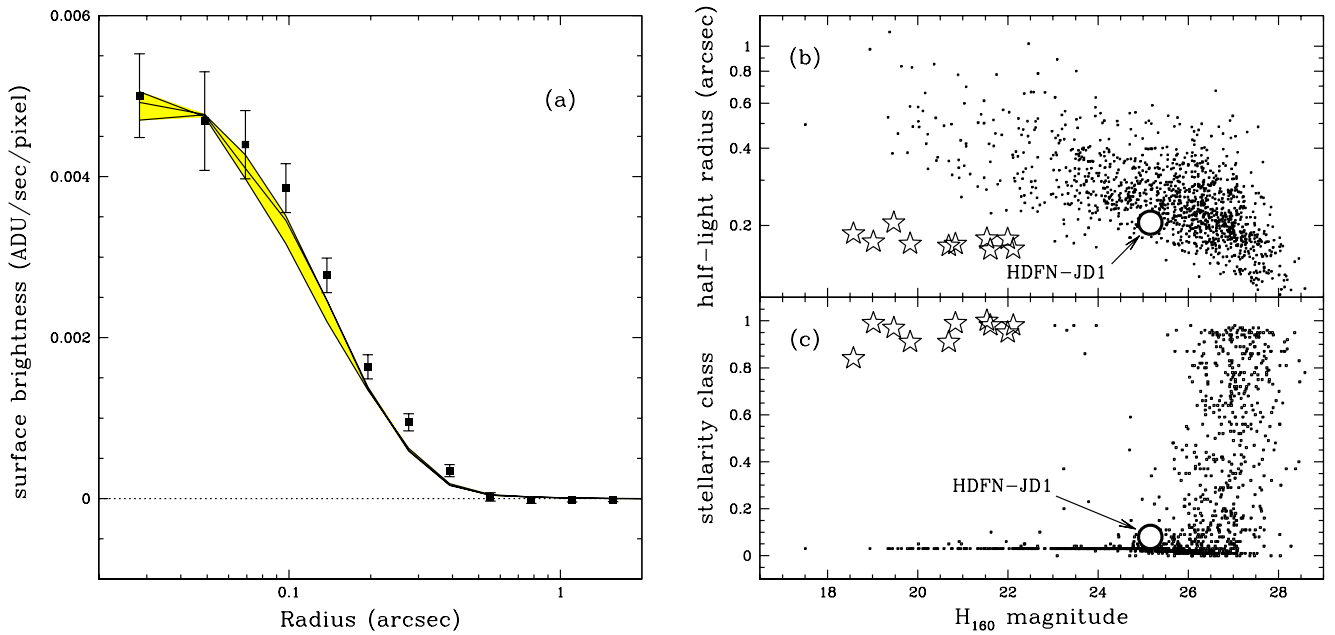


Fig. 4.— *Left:* (a) Radial surface brightness profile of HDFN-JD1 (points) compared to three faint, isolated HDF stars (lines, shaded region) which have been registered and scaled by non-negative cross-correlation. *Right top:* (b) H_{160} half light radius vs. magnitude for HDF objects. Known stars are indicated by star symbols, and HDFN-JD1 is labeled. *Right bottom:* (c) SExtractor stellar classifier (at H_{160}) for HDF objects, with symbols as in (b).

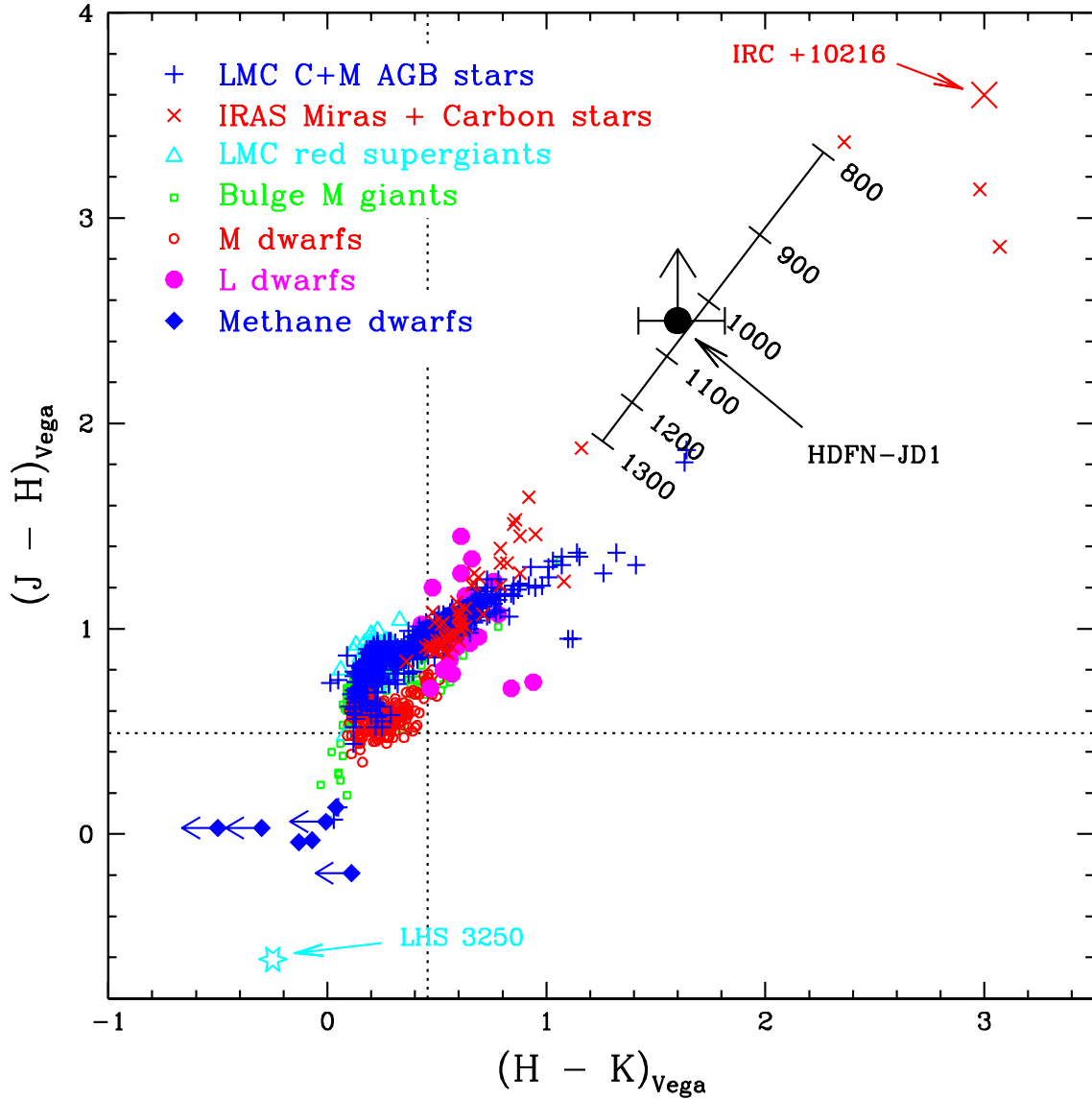


Fig. 5.— $J - H$ vs. $H - K$ color-color diagram (on the conventional, Vega-normalized system) comparing HDFN-JD1 to a variety of cool or reddened stars. The NICMOS photometry has been converted to standard infrared magnitudes using synthetic color corrections, and is plotted as a 2σ lower limit in $J - H$. The dotted lines mark the colors of a flat f_ν spectrum (i.e., zero AB colors). The stellar data are taken from Frogel, Mould & Blanco 1990 and Costa & Frogel 1996 (LMC AGB stars), Whitelock *et al.* 1994, 1995 (IRAS Miras and carbon stars), Oestreicher, Schmidt-Kaler, & Wargau 1997 (supergiants), Frogel *et al.* 1990 (M giants), Leggett 1992 and Leggett *et al.* 1998 (M dwarfs), Kirkpatrick *et al.* 1999 (L dwarfs), and Burgasser *et al.* 1999, Leggett *et al.* 1999, and Strauss *et al.* 1999 (methane dwarfs). IRC+10216 (Becklin *et al.* 1969) is also shown, along with LHS 3250 (Harris *et al.* 1999) which is believed to be a very cool DC white dwarf. The solid track shows the colors of a black body with labeled temperatures (in K).

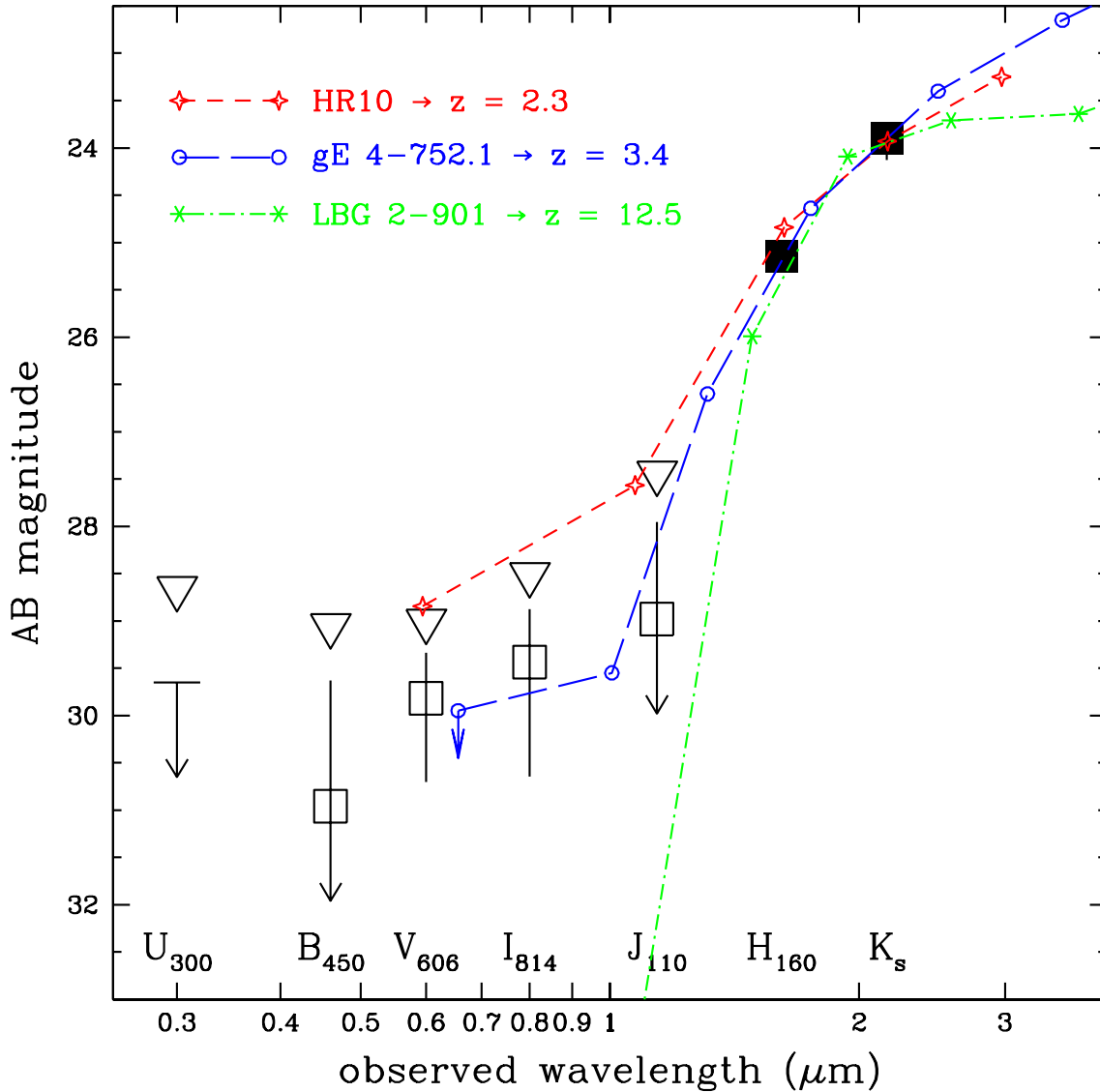


Fig. 6.— Spectral energy distribution (SED) of HDFN-JD1. Open squares mark measurements with $S/N < 2$. Error bars ($\pm 1\sigma$) are superimposed, except when $S/N < 1$, where the downward error bar is shown as an arrow. Triangles mark 2σ magnitude limits for U_{300} through J_{110} . Three SEDs of other, real galaxies, artificially redshifted and normalized to the K_s flux of HDFN-JD1, are superimposed for comparison: the dusty galaxy HR10 shifted to $z = 2.3$, the HDF giant elliptical galaxy 4-752.1 shifted to $z = 3.4$, and the HDF Lyman break galaxy 2-901 shifted to $z = 12.5$. For the latter, the flux point shortward of Lyman α has been reduced to account for the assumed opacity increase of the Lyman α forest at $z = 12.5$, and flux shortward of the Lyman limit has been set to zero. For HDF 4-752.1, the shortest wavelength measurement (from the HDF U_{300} image) probably overestimates the real UV flux from the gE galaxy because of a red leak in the WFPC2 F300W filter; this is indicated by a downward-pointing arrow. All three SEDs are qualitatively similar to that of HDFN-JD1.

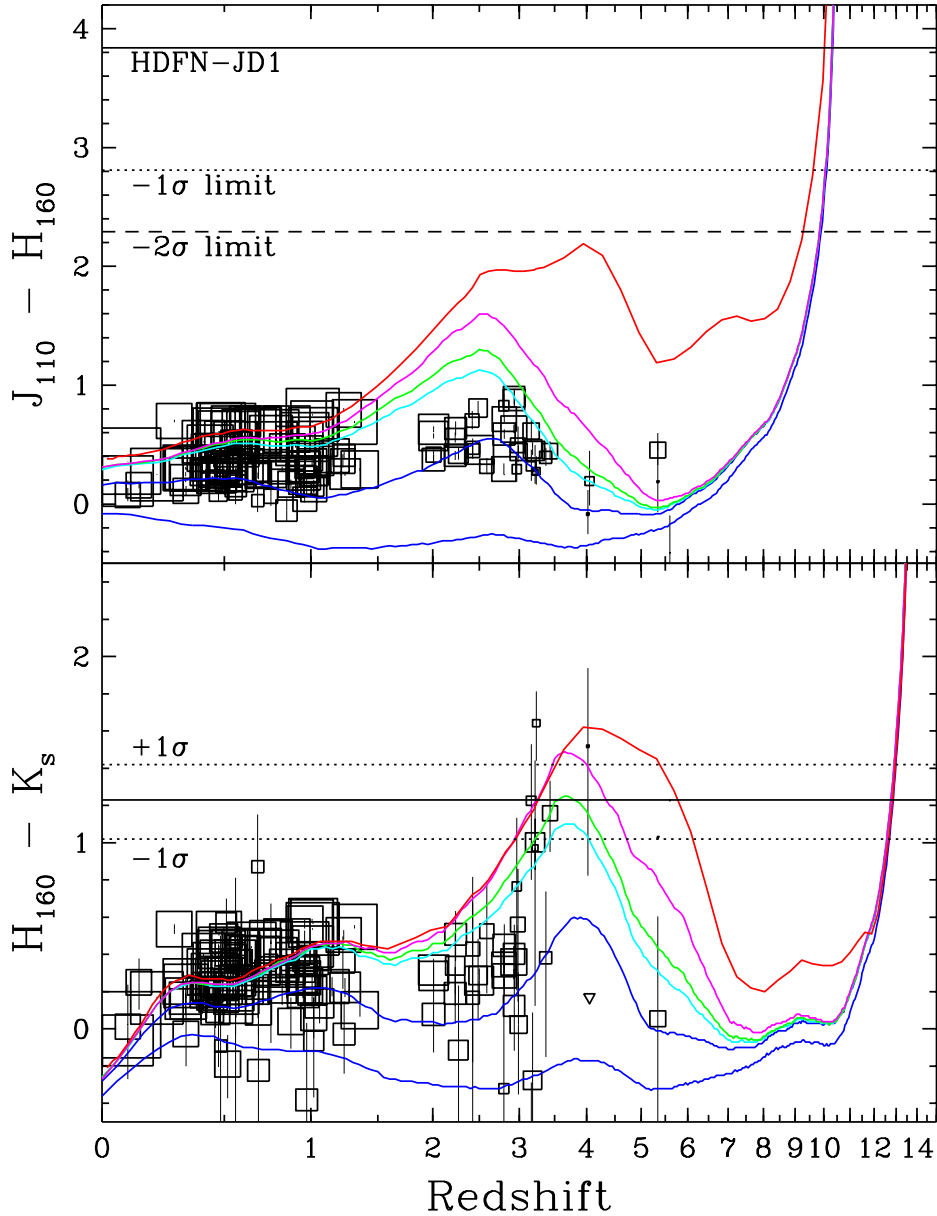


Fig. 7.— Infrared colors (on the AB system) versus redshift for galaxies with spectroscopic redshifts in the HDF-N. Point sizes scale with the H_{160} magnitudes. The solid horizontal lines mark the nominal colors of HDFN-JD1, and the dotted lines mark the 1σ uncertainties for $H_{160} - K$ and lower color limit for $J_{110} - H_{160}$; the dashed line for $J_{110} - H_{160}$ marks the 2σ lower color limit. The curves show the expected colors of various model galaxy types. The reddest of these is a Bruzual & Charlot (1996) model for an elliptical galaxy formed at $z = 15$ in a 10^8 year burst and evolving passively in a cosmology where $\Omega_M = 0.3$, $\Omega_\Lambda = 0.7$, and $H_0 = 70 \text{ km s}^{-1} \text{ Mpc}^{-1}$. The other curves are unevolving models matching the colors of local spirals and unreddened starburst galaxies. The evolving elliptical model matches the $H_{160} - K$ color of HDFN-JD1 at $3 \lesssim z \lesssim 6$, but never quite reaches the 2σ limit on $J_{110} - H_{160}$. The HI opacity of the intergalactic medium has been included by extrapolating the models of Madau (1995) to $z = 15$. At these large redshifts, the IGM transmission is effectively a step function at Lyman α . Redshifts were compiled from Cohen *et al.* (1996), Steidel *et al.* (1996b), Lowenthal *et al.* (1997), Dickinson (1998), Weymann *et al.* (1998) and Spinrad *et al.* (1998).